E3S Web of Conferences **40**, 05033 (2018) https://doi.org/10.1051/e3sconf/20184005033
River Flow 2018

Experimental study of the surface oscillations induced by a shallow flow past a lateral cavity

L. Engelen[1,*], *S.* Creëlle[1], *L.* Schindfessel[1], and *T.* De Mulder[1]

[1]Hydraulics Laboratory, Dept. of Civil Engineering, Ghent University, Belgium

Abstract. The present work presents an experimental study in which resonant surface oscillations inside a lateral cavity are reconstructed, often denoted as seiching, which are excited by a shallow main stream flowing past the horizontal basin. Firstly, the flow configurations that trigger transverse and/or longitudinal seiching are studied using pressure measurements in the corners of the cavity, which shows that a transitional Froude number exists, approximately 0.63, at which the dominant seiching mode changes from transverse to longitudinal seiching. For both types of resonant conditions, the surface shape is analyzed in detail using a three-dimensional particle tracking velocimetry (3D-PTV) setup. Based upon floating seeding particles, the 3D surface is reconstructed with a superior spatial resolution compared to traditional measurement techniques, which confirms the multimodal aspect of the surface oscillations.

1 Introduction

1.1 Background

This paper is devoted to open-channel shallow flow past a lateral cavity, i.e. a (rectangular) horizontal embayment of which one side is connected with a coastal or fluvial main stream. Such embayments are encountered in various natural (oxbows, cut-off meanders) and artificial (ports, groyne fields, etc.) configurations. In [1], it was shown that the flow field inside the cavity is characterized by one or multiple counter-rotating large-scale recirculation cells, depending on its width-to-length ratio W/L. For a square cavity with W/L=1 (as in the present case), a single main gyre occupies almost the whole of the cavity area.

The strong velocity gradient between the main stream and the low-velocity area inside the cavity generates a shear layer at their interface. This mixing layer transfers mass and momentum towards the cavity and is dominated by coherent structures, i.e. Kelvin-Helmholtz vortices with a vertical axis of rotation that are generated at the upstream corner. These quasi-periodic eddies are then advected downstream along the mixing layer and finally impinge on the downstream corner. There, the eddies' kinematic energy is transformed into potential energy, which causes a (fluctuating) rise of the local water level at the stagnation point and a fluctuating inflow towards the cavity.

Free surface oscillations with important amplitudes can be generated by multiple (hydrodynamic and meteorological) excitation mechanisms. Such surface conditions should be

*e-mail: Lukas.Engelen@UGent.be

avoided to ensure safe navigation and loading/unloading of ships present inside the basin. This paper is devoted to one of the less known sources of surface oscillations, named seiching, in which large standing gravity waves within the cavity in the transverse and/or longitudinal direction are excited for certain combinations of cavity geometry and main channel flow. Moreover, in [2], seiching was reported to increase mass transfer between the main stream and the cavity by 40%. In a real river system, this would result in more exchange of e.g. sediments, pollutants or nutrients and, as such, disturb the ecological equilibrium. Additionally, the increased mass transfer could result in a reduction of the local (navigable) water depth and require more maintenance dredging. Given its ecological and economical impact, understanding the origin and impact of seiching is important.

Previous research [2–5] suggested that seiching is triggered when the natural frequency of the cavity is in agreement with the eddies passing frequency, while [2, 6] found that also the flapping or 'jitter' phenomenon of the shear layer (Figure 1) is in phase with the surface oscillations. Nonetheless, it remains difficult to predict when seiching will occur. Moreover, most authors only reported the first mode of seiching (n=1 in Section 3.1) according to either the transverse or longitudinal direction, in which they assumed a uni-directional sinusoidal surface shape. However, [5] showed that multiple seiching modes can be present simultaneously, giving rise to bidirectional and multimodal seiching in both the transverse and longitudinal direction.

It is evident that the analysis of such complex flow configurations requires a detailed description of the time-dependent surface shape. Superior to the limited spatial resolution of traditional point-based (e.g. ultrasonic [5] or pressure [2]) measurements, three-dimensional particle tracking velocimetry (3D-PTV) will in this paper be employed to reconstruct the entire 3D cavity surface during seiching. Although the technique is currently still being optimized, the preliminary results presented in this paper show that it is able to give a good approximation of the 3D surface shape. Additionally, the Lagrangian methodology results automatically in a description of the (surface) flow field and provides a (first) indication of the mass transfer between the cavity and main channel. Although this paper is limited to a description of the surface shape inside the cavity, these features of the technique will be exploited in future research.

1.2 Objectives

The aim of the present paper is two-fold. First, an experimental study is presented in which the presence and relative magnitude of the different seiching modes are quantified for a range of flow conditions using two simultaneous pressure registrations. Although previous research showed that the possible frequency of the cavity oscillations can be estimated based on the cavity's geometry and water depth, no method has been found to predict when and which mode will be triggered.

Secondly, 3D-PTV is used to reconstruct the surface shape for two flow configurations with dominant seiching in either the transverse or longitudinal direction. Compared to traditional single-point surface measurements, the high spatial resolution of the presented 3D-PTV implementation is ideally fitted to capture the complex 3D surface dynamics and distinguish the different seiching modes.

2 Experimental setup

2.1 Laboratory facility

The experiments were performed in the 90°angled confluence flume at the Hydraulics Laboratory of Ghent University (Figure 1), of which both the main channel and tributary channel

have a width $b = 0.40$ m. In the tributary, a water retaining wall was installed to create a lateral, square cavity with a length L and width W equal to 0.40 m, hence an aspect ratio $W/L = 1$. The water surface in the cavity was studied for a large range of flow conditions, for which the discharge Q in the incoming main channel was varied between 7.5 and 45.0 l/s. The mean water depth inside the cavity h_m was determined as the average of the local time-averaged pressure registrations (see Section 2.2), $h_m = (\overline{h_{P1}} + \overline{h_{P2}})/2$, and varied between 5.0 cm and 14.1 cm. Based on the corresponding bulk velocity in the main channel $U_b = Q/(bh_m)$, the non-dimensional Froude and Reynolds numbers are defined as $Fr = U_b/\sqrt{gh_m}$ and $Re_h = U_b h_m/\nu$, in which the kinematic viscosity of water ν equals $1.0035 \times 10^{-6}\, m^2/s$ for water at 20 °C. For the present experiments, $Fr = 0.19 - 0.68$, similar to the previous research but relatively large compared to field conditions, and $Re_h = 10,600 - 112,200$.

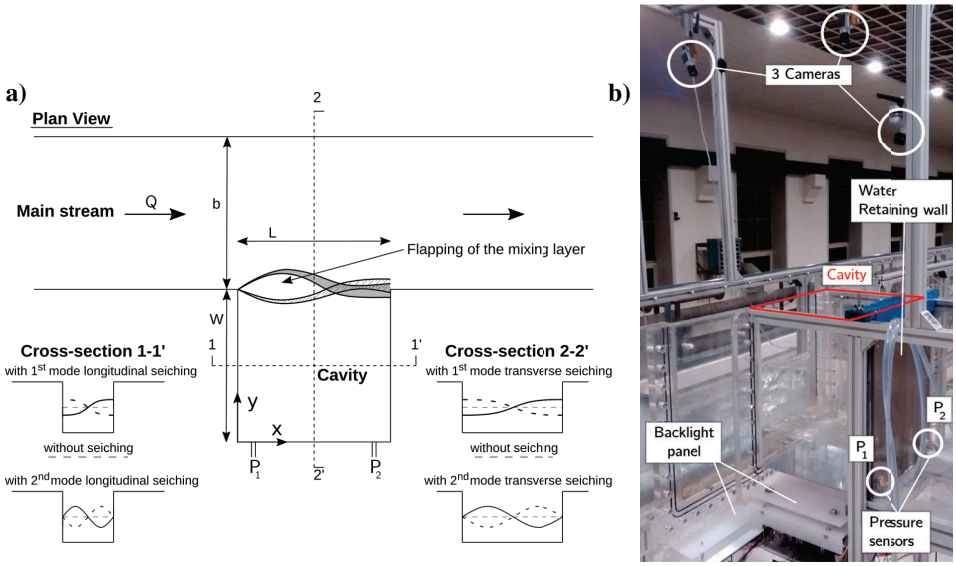

Figure 1. Schematic sketch (a) and photograph (b) of the experimental setup. The location of the upstream (P_1) and downstream (P_2) inlets of the pressure sensors in the water retaining wall are indicated, as well as the position of the cameras and backlight panel for 3D-PTV. The first two theoretical seiching modes in both the longitudinal (x-) and transverse (y-) direction are shown for cross-section 1-1' and 2-2', respectively.

2.2 Measurement techniques

Two pressure sensors (UNIK5000 of GE Measurement & Control), installed near the respective edges of the water retaining wall (P_1 and P_2 in Figure 1), were used to acquire simultaneous measurements of the local surface level with a measurement accuracy of ±0.05 mm over a period of 150 s and a sampling frequency of 20 (Section 3.2) or 25 Hz (Section 4). By positioning the two pressure sensors near the respective edges of the retaining wall, the phase difference between both signals allowed to distinguish the first mode of longitudinal seiching from transverse seiching.

Secondly, a recently developed three-dimensional particle tracking velocimetry (3D-PTV) setup was in this paper adopted to reconstruct the 3D shape of the oscillating water surface. 3D-PTV is an image-based Lagrangian velocity measurement technique, in which

the individual paths of small particles are tracked using multiple cameras to determine their 3D positions. This technique was already applied in cavity research by [6] using neutrally-buoyant particles, although the present results were obtained by tracking positively buoyant polyethylene particles at the surface ($\rho = 0.9\ \mathrm{g/cm^3}$ and diameter ≈ 3 mm). These floating particles avoided the complication of refraction (as in [6]) and eliminated the need for a (laser) light sheet to selectively illuminate the sampling area. This reduced the costs of the experimental setup and allowed to gain experience with 3D-PTV prior to future improvements of the setup. The size of the adopted particles was relatively large, which would for regular PTV applications (velocity measurements) have a negative influence on the particle inertia and response characteristics. However, since the particles were in this paper only used to reconstruct the 3D surface shape, their relatively large size does not limit the accuracy of the presents results.

Images were acquired with three synchronized CMOS sensor cameras (8 Bit, 960 x 480 pixels) positioned above the flume, at a frame rate of 25 Hz and a shutter speed of 1/1000 s over a time span of 4 min in total. During the experiments, the bottom of the flume was lit from below by a uniform LED backlight panel (Figure 1b) to avoid specular reflections and maximize the camera frame rate while maintaining good image contrast. Prior to the experiments, the cameras were calibrated to correct for lens aberration and obtain an estimate of the intrinsic camera parameters using OpenCV [7]. The 3D reconstruction of the particle positions was done using the open-source library OpenPTV [8], initially developed at ETH Zürich [9], which is able to reconstruct the 3D trajectories through spatial and temporal stereoscopic matching.

3 Identification of the cavity's seiching modes

3.1 Theoretical expectations

In a (semi-)enclosed basin, long-period standing surface oscillations can occur when the forcing frequency equals the natural frequency of the basin. When such standing gravity waves occur in (relatively shallow) harbors and lakes, they are often called seiches [10]. When the water depth is small compared to the length of the basin, the Merian formula [11] can be used to predict the possible seiche frequency f_n based upon a characteristic length L_s (in the direction of seiching) and the average water depth in the basin h_m:

$$f_n = \frac{n\sqrt{gh_m}}{2L_s} \tag{1}$$

in which n indicates the mode of the seiching, equal to the amount of nodes of the sinusoidal surface shape and g is the gravitational acceleration.

The experiments of [5] showed that seiching in a square cavity is possible in both the longitudinal and transverse direction, of which the first two modes (n=1,2) are shown in Figure 1a. For the present geometry, the corresponding frequencies are computed with eq. (1) and $L_{s,L} = L$ and $L_{s,T} = b + W = 2W$ for seiching in the longitudinal and transverse direction, respectively. Since $L = W(= b)$, substitution of $L_{s,T} = 2\,L_{s,L}$ in eq. (1) implies that, for the experiments in this paper, the natural frequencies of transverse seiching are half of the longitudinal frequencies. As a consequence, some higher modes of transverse seiching (n>1) will have the same period as the longitudinal modes (e.g. $f_{T,2} = f_{L,1}$). Although it will be shown that the combination of two (single-point) measurements is sufficient to distinguish transverse from longitudinal seiching, these overlapping frequencies motivate the use of 3D-PTV in which the entire surface shape is determined.

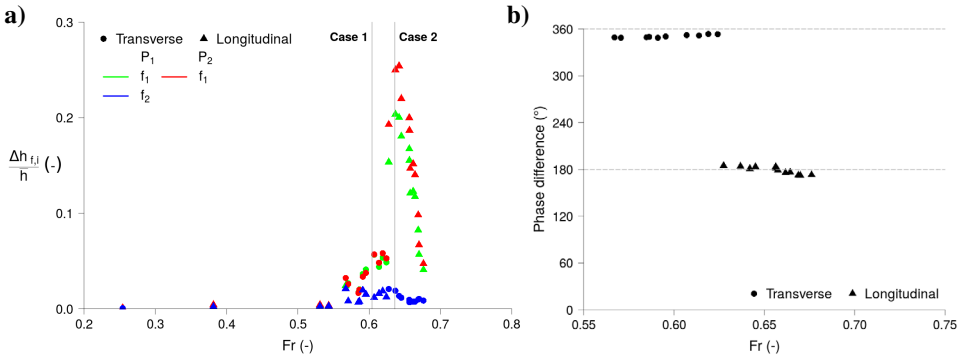

Figure 2. In function of the Froude number: a) Non-dimensional amplitude of the dominant seiching mode(s) of P_1 (green and blue) and P_2 (red), with vertical lines indicating the two analyzed cases of Section 4; b) Phase shift of the dominant mode of seiching (f_1) determined by means of the cross-spectrum of both signals for flow configurations with significant seiching ($Fr > 0.55$).

3.2 Experimental results

Based on the individual recordings of pressure sensors P_1 or P_2 (during a time span of 150 s at 20 Hz), the normalized amplitude spectra of the local water depth variations were used to estimate the magnitude of the surface oscillations corresponding to the peaks in the spectrum. In Figure 2a, the frequencies with the maximum and second largest amplitude are indicated by f_1 and f_2 respectively, while the corresponding amplitude is denoted Δh_{f_i} and is determined for every pressure sensor separately. The latter is made dimensionless by the local time-averaged water depth $\overline{h}$ for the time period of the pressure registrations (150 s). The mode of seiching at the dominant frequency was determined based on the cross-spectrum of both signals evaluated at f_1 (Figure 2b). Given the symmetrical positioning of the pressure sensors inside the cavity, the first-modes (n=1) of transverse (•) and longitudinal seiching (▲) are characterized by a phase difference of 360°and 180°, respectively.

3.3 Discussion

Figure 2b shows that for Fr<0.63, the recorded pressure oscillations of P_1 and P_2 are approximately in phase. This indicates that the most dominant oscillations in the cavity correspond to transverse seiching. At $Fr = 0.63$, the phase difference evaluated at f_1 suddenly changes to 180°, suggesting that the surface oscillates in the longitudinal cavity direction (according to n=1). Additionally, Figure 2a suggests that the amplitude of longitudinal seiching is somewhat higher at the downstream corner, while this difference is not observed for transverse oscillations. This observation is most probably caused by the impingement of the oscillating shear layer at the downstream corner, which has more kinetic energy during longitudinal seiching due to the higher flow velocity (and Fr). Since the latter is periodically transformed into potential energy, the higher Fr numbers explain the enhancement of the surface variation at the downstream end of the cavity (P_2). Due to friction, this local enhancement of the incoming flow is damped and thus becomes less significant at the upstream position of P_1.

In contrast to P_2, the surface variation at P_1 will only minimally be affected by the impingement of the shear layer. Therefore, the pressure series of P_1 are considered representative for the large-scale cavity oscillations (seiching) and are used to compare the amplitude of the second largest peak in the amplitude spectrum (f_2) with the dominant mode of seiching

(f_1). Figure 2a shows that below $Fr = 0.63$, transverse seiching (n=1) dominates the cavity surface, of which the amplitude corresponding to the dominant frequency f_1 has a maximum of approximately 6% of $\overline{h}$. The amplitude of the second largest peak in the amplitude spectrum, corresponding to longitudinal seiching (n=1), remains relatively low ($\approx$ 1.5% of $\overline{h}$). At $Fr = 0.63$, a sharp change of the surface is noticed, with oscillations in the longitudinal direction (n=1) that increase up to 20% of the mean water depth and a decrease of the transverse oscillations to $\Delta h_{f_1}/\overline{h} \approx 1\%$. Therefore, it seems that below $Fr = 0.63$, the multimodal aspect of seiching is more pronounced, while for $Fr > 0.63$ the surface behaves almost perfectly sinusoidal in the longitudinal direction. This transitional value at $Fr = 0.63$ seems to be confirmed by the literature, in which transverse (e.g. [6, 12]) and longitudinal (e.g. [2], [3]) seiching was observed below and above $Fr = 0.63$, respectively.

4 Detailed study of the surface shape during seiching

In the following, the 3D surface variations of two flow cases of Section 3.2 (indicated in Figure 2a) are studied more in detail using 3D-PTV, of which the results will be verified by simultaneous pressure registrations. During flow case 1, $h_m/L = 0.19$, $Re = 40,400$ and $Fr = 0.60 < 0.63$, and dominant transverse seiching (n=1) with $f_1 = 0.50$ Hz was observed. During flow case 2, $h_m/L = 0.29$, $Re = 78,800$ and $Fr = 0.64$, which resulted in dominant longitudinal seiching (n=1) with $f_1 = 1.26$ Hz.

To compare the single-point pressure measurements with the scattered particle cloud obtained with 3D-PTV, an estimate of the water depth based on the 3D-PTV results was determined at the location of P_1 and P_2. First, a linear plane surface was fitted to the entire point cloud, which proved robust against some spurious particle positions. Wrongly detected outliers were then removed by setting a threshold on the deviation between their elevation and their estimated position using the linear surface model. Subsequently, a more suitable surface model was adopted to obtain a more accurate representation of the instantaneous surface shape, in which the linear model was extended with a sinusoidal term in the direction of the expected seiching mode (transverse or longitudinal). Finally, the estimated water depths at the location of P_1 and P_2 according to the fitted model were compared with the simultaneous pressure-based water depths.

4.1 Case 1: transverse seiching

Figure 3a gives a comparison between the simultaneous measurements of the pressure sensors and the estimated water depths according to the fitted surface model at P_1 and P_2. For both, the instantaneous water depth is presented in a dimensionless way, relative to the local time-averaged water depth $\overline{h}$. Firstly, it can be seen that the results obtained with the pressure sensors and 3D-PTV follow the same sinusoidal trend. However, the water depth estimated with the fitted surface model seems to show a more irregular, peaked behavior. The latter is most probably caused by the combined effect of non-linear surface fitting and the uncertainty of the 3D particle positions. However, the difference between the pressure-based and 3D-PTV results is considered acceptable and sufficient to describe the surface reliably. Secondly, both the pressure-based and 3D-PTV-based water depth variation at P_1 and P_2 oscillate approximately in phase. Given the positioning of the pressure sensors, this confirms that the cavity is dominated by first-order transverse seiching.

Figure 3b gives the dimensionless ($\frac{h-\overline{h}}{\overline{h}}$) particle positions and corresponding fitted surface model for two instances in time with a time difference $T_{T,1}/2 = 1/(2f_{T,1})$, for which the maximum deviations with respect to the mean water depth are large. These fitted surface

models confirm the sinusoidal shape of the surface in the transverse (y-) direction, with a node approximately at the interface between cavity and main channel. However, even though mostly inclined in the y-direction, both fitted surfaces also have a small longitudinal inclination (x-direction). Therefore, the 3D surface reconstruction obtained with 3D-PTV suggests that the cavity surface is the superposition of both transverse and longitudinal seiching modes. Moreover, it can be seen that the deviation from the mean water depth ($h = \overline{h}$) is most pronounced at the downstream wall, which confirms the statement in Section 3.3 regarding the local enhancement of the surface variations due to impingement of the shear layer.

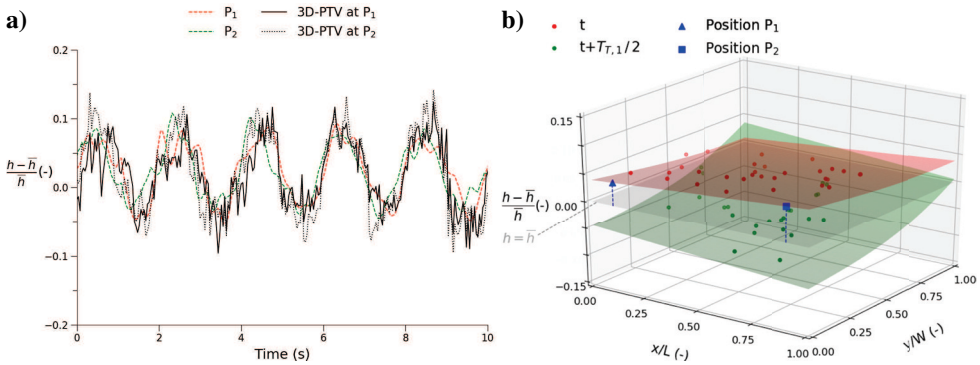

Figure 3. Case 1: a) Small part (10 s) of the recorded surface variation; b) 3D reconstruction of two instantaneous views (detected particles and fitted surface model) with a time difference equal to $T_{T,1}/2$.

4.2 Case 2: longitudinal seiching

Figure 4a shows a comparison between the pressure series and the results obtained with the fitted surface model using a sinusoidal term in the longitudinal direction for case 2 (dimensionless by $\frac{h-\overline{h}}{\overline{h}}$). Compared to case 1, the larger amplitude and higher frequency of longitudinal seiching made a reliable tracking of the particles more difficult. Additionally, it was noticed that the particles in case 2 tended to be centered in the low-velocity region in the center of the cavity, providing less distributed information for the global optimization. Nonetheless, the image-based and pressure-based results show the same trend, in which the oscillations at P_1 and P_2 have a phase difference of $\approx 180°$.

Figure 4b represents two instantaneous views of the dimensionless water depth inside the cavity with a time difference $T_{L,1}/2 = 1/(2f_{L,1})$. The fitted surfaces seem to match very well with the expected sinusoidal surface shape and seem less affected by multimodal seiching compared to case 1. This could be expected, since Figure 2a showed that the relative magnitude of f_1 is much more pronounced compared to f_2 in case of longitudinal seiching. Nonetheless, the green-colored surface in Figure 4b still has a small inclination in the transverse y-direction, indicating a limited contribution by the transverse seiching mode(s).

5 Conclusion

This paper has presented a detailed experimental study of the surface oscillations inside a lateral cavity during seiching conditions. Firstly, the type and magnitude of the seiching modes were quantified for multiple flow configurations using two pressure sensors positioned at opposite sides of the cavity. This suggested that there exists a transitional Froude number around 0.63, at which the most dominant mode changes from transverse to longitudinal seiching for

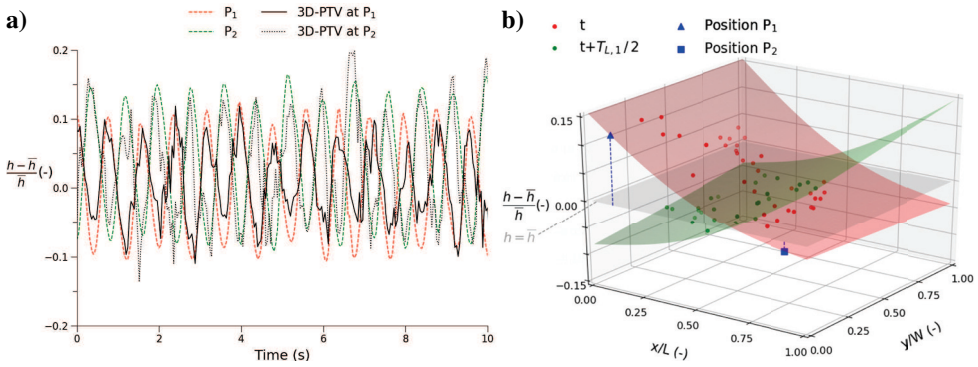

Figure 4. Case 2: a) Small part (10 s) of the recorded surface variation; b) 3D reconstruction of two instantaneous views (detected particles and fitted surface model) with a time difference equal to $T_{L,1}/2$.

the same square cavity geometry. Moreover, the relative amplitude of longitudinal seiching proved more pronounced than that of transverse seiching.

Secondly, two flow cases with either dominant transverse or longitudinal (first-order) seiching were analyzed using the high spatial and temporal resolution of a recently developed 3D-PTV setup. Although the technique is still being optimized, the preliminary results in this paper seem to confirm the multimodal and bidirectional aspect of the seiching phenomenon. Especially in case of dominant transverse seiching ($Fr < 0.63$), the surface seems to be the superposition of multiple seiching modes.

Further research will focus on the improvement of the 3D-PTV setup to achieve better and more robust results. Subsequently, 3D-PTV will not only be used to analyze the surface oscillations even more in detail, but the Lagrangian information will also be used to study the flow field and mass exchange between the main stream and cavity.

6 Acknowledgments

The first author is a Ph.D. fellow of the Special Research Fund (BOF) of Ghent University.

References

[1] N. Riviere, M. Garcia, E. Mignot, G. Travin, *Characteristics of the recirculation cell pattern in a lateral cavity*, in *Proc. Int. Conf. Fluv. Hydraul., IAHR* (2010), pp. 673–679
[2] B. Tuna, E. Tinar, D. Rockwell, Exp. Fluids **54**, 1586 (2013)
[3] I. Kimura, T. Hosoda, J. Hydraul. Eng. **123**, 98 (1997)
[4] M. Wolfinger, C. Ozen, D. Rockwell, Phys. Fluids **24**, 104103 (2012)
[5] E. Mignot, M. Pozet, N. Riviere, S. Chesne, *Bidirectional seiching in a rectangular, open channel, lateral cavity*, in *Proc. 22ème CFM, Lyon, France (FR)* (2015)
[6] Y. Akutina, Ph.D. thesis, McGill University (2015)
[7] G. Bradski, Dr. Dobb's Journal of Software Tools (2000)
[8] Consortium, OpenPTV, *Openptv*, `http://www.openptv.net/`
[9] J. Willneff, Ph.D. thesis, ETH Zurich, Switzerland (2003)
[10] A.B. Rabinovich, in *Handbook of coastal and ocean engineering* (World Scientific, 2010), pp. 193–236
[11] K. VonderMühll, Mathematische Annalen **27**, 575 (1886)
[12] B. Tuna, D. Rockwell, J. Fluid Mech. **758**, 655 (2014)